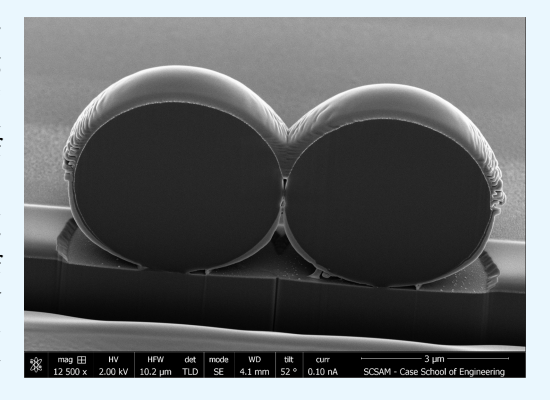


# Local Measurement of Janus Particle Cap Thickness

Aidin Rashidi,<sup>†</sup> Marola W. Issa,<sup>†</sup> Ina T. Martin,<sup>‡</sup> Amir Avishai,<sup>§</sup> Sepideh Razavi, <sup>||</sup> and Christopher L. Wirth\*, To

Supporting Information

ABSTRACT: Janus particles have anisotropy in surface chemistry or composition that will effect dynamics and interactions with neighboring surfaces. One specific type of Janus particle is that consisting of a native micrometer-scale particle with a cap of gold, platinum, or another metal deposited with a typical thicknesses of ~10 nm. A key characteristic of metal-capped Janus particles prepared with glancing angle deposition is the cap thickness. The nominal thickness is usually assumed to be uniform across the cap for modeling or interpretation of data, but the vapor deposition fabrication process likely does not produce such a cap because of the particle's curvature. These nonuniformities in the cap thickness may have a profound impact on Janus particle dynamics at equilibrium and in response to external fields. Herein, we summarize an experimental technique that utilizes focused ion beam slicing, image analysis, and results for the direct and local measure of cap thickness for 5  $\mu$ m polystyrene



spheres with a gold cap of nominal thicknesses of 10 or 20 nm. We found the cap varied in thickness continuously along the perimeter of the particle and also that the deposition rate, varying between 0.5 and 2.0 Å/s, did not significantly alter the way in which the thickness varied. These data support the hypothesis that cap thickness of a Janus sphere will vary across the gold surface contour, while demonstrating a feasible route for direct measurement of Janus particle cap thickness.

KEYWORDS: anisotropy, glancing angle deposition, Janus particles, cap thickness, focused ion beam

anometer- to micrometer-scale particles with chemical or geometric anisotropy have the potential to transform applications in chemical and physical sensing, medical drug delivery, as analogues for molecular scale phenomena, and in consumer products.<sup>1-9</sup> One such anisotropic particle is a patchy or "Janus" particle, typically consisting of a native colloidal sphere with a cap of a second material covering approximately half of the available surface area. Other particles, including rods 10 and sheets, 11 can also be made Janus with a variety of synthetic routes. Janus particles have been identified as good candidates for sensing in complex rheological or mechanical environments because of the optical signature inherent in a Janus particle, which facilities tracking the rotational or translational diffusion of the particle. Janus particles with engineered ligand surface chemistries may offer a strategy for directed cell entry that particles of uniform chemistry or shape do not. Further, foams and emulsions stabilized by particles that act as solid surfactants are extremely stable. 12-14 Regularly found in consumer products and food, these multiphase fluids would benefit from technology that results in long shelf life and other added value functionalities to products. 15 Engineered Janus particles could have a significant

impact on advancing technologies based on particle-stabilized multiphase fluids.

One route for fabricating Janus particles is to conduct vapor deposition of a cap material onto a monolayer of native particles. 16 Vapor deposition and subsequent chemical modification were initially used to fabricate Janus particles, with ~50% area coverage, but were developed further into a robust technique called glancing angle deposition (GLAD) capable of fabricating particles with patches of various areas and geometry. 17,18 GLAD is now regularly used to produce patchy colloids of varying native particle and patch composition, surface area, and geometry. 19 The nominal patch or "cap" thickness is typically controlled by the instrument used for the deposition process, whereas the cap size and shape is controlled by adjusting the substrate inclination angle and the angle with respect to the crystallinity axis. Scanning electron microscopy is effective for measuring

Received: July 2, 2018 Accepted: August 24, 2018 Published: August 24, 2018

<sup>&</sup>lt;sup>†</sup>Chemical and Biomedical Engineering, Cleveland State University, Cleveland, Ohio 44115, United States

<sup>\*</sup>Materials for Opto/Electronics Research and Education (MORE) Center, Case Western Reserve University, Cleveland, Ohio 44106, United States

<sup>§</sup>Swagelok Center for Surface Analysis of Materials, Case Western Reserve University, Cleveland, Ohio 44106, United States Chemical, Biological, and Materials Engineering, University of Oklahoma, Norman, Oklahoma 73019, United States

**ACS Applied Materials & Interfaces** 

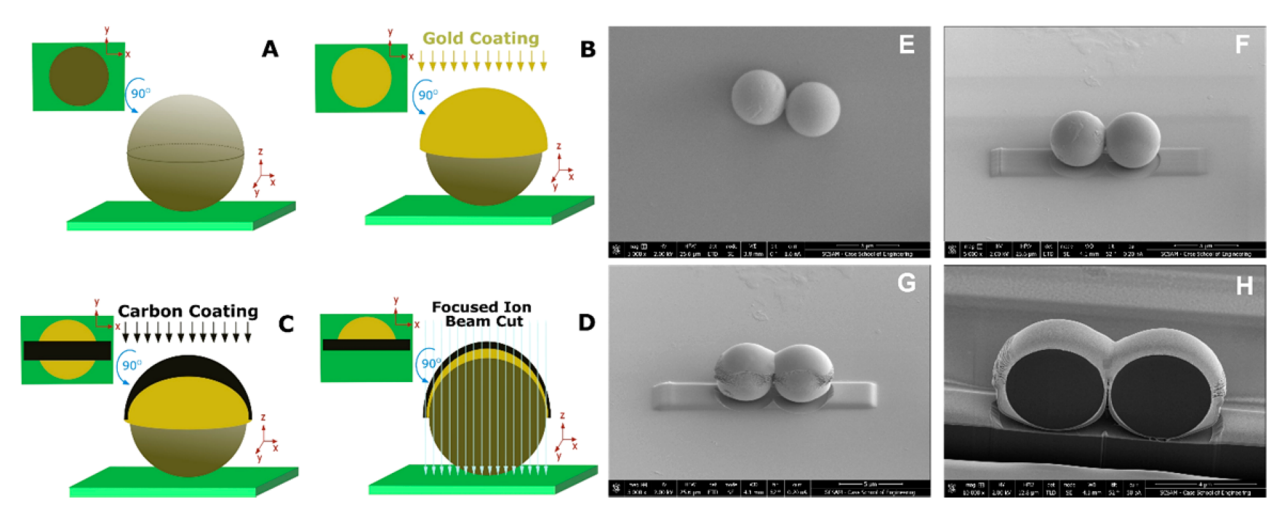


Figure 1. Preparation of a cross-section of a Janus sphere. The process consisted of (A) depositing a native polystyrene particle, (B) gold deposition in the direction normal to the substrate, (C) local carbon coating in a strip along the particle and normal to the substrate, and (D) a focused ion beam (FIB) cut normal to the substrate to reveal the particle's cross-section. The process was imaged to show doublets following (E) gold deposition (top view), (F) local carbon deposition (angled view), (G) the first FIB cut (angled view), and (H) the final FIB cut, revealing the cross section of the doublet (angled view).

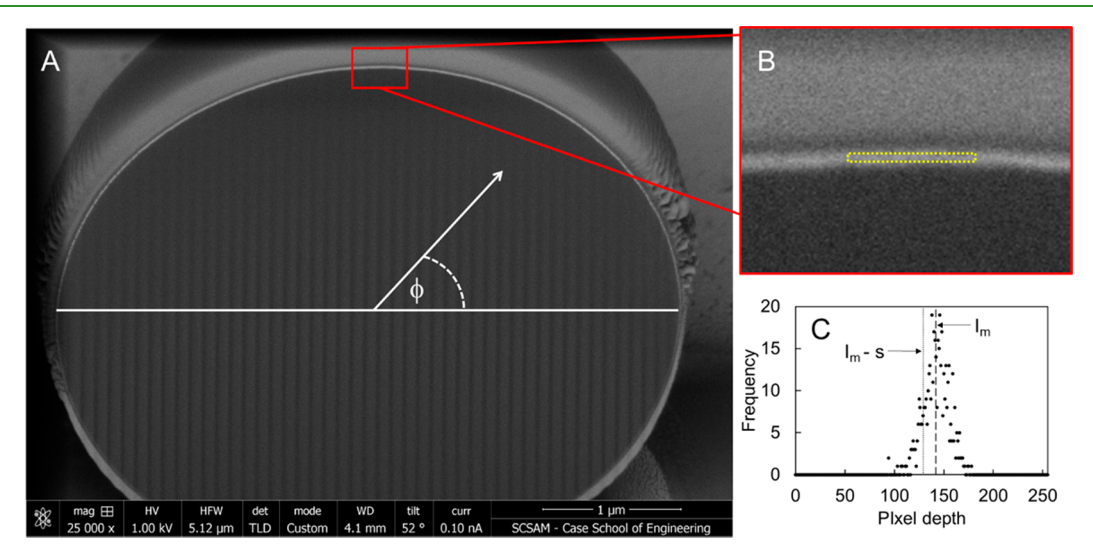


Figure 2. Determining threshold value for image processing. The threshold value was set equal to the difference between the mean and standard deviation of a selection of pixels along the gold contour of the particle. The pixels used to calculate these values were selected from contour positions  $\phi = 135^{\circ}$ , 90°, and 45°. (A) Original SEM micrograph, (B) zoomed in image and location of pixels used for calculation at  $\theta = 90^{\circ}$ , (C) histogram of intensities from selection with pixel depth mean  $(I_{\rm m})$  and standard deviation (s) at  $\theta = 90^{\circ}$ . The threshold used for image analysis was determined from the mean and standard deviations of data obtained at  $\phi = 135^{\circ}$ , 90°, and 45°. Images were thresholded by making all pixels with  $>I_{\rm m}$ -s equal to a pixel depth of 255.

the cap surface area and geometry, but there is currently no practical method for measuring cap thickness. The cap thickness is typically assumed to be equal to the nominal thickness along the entire cap contour. However, the real cap thickness, as well as the variation of the thickness along the contour of the cap, is important for predicting and interpreting the dynamics of patchy colloids at equilibrium in response to external fields or swimming in response to local physiochemical gradients.

Herein, we report the first local measure of cap thickness for Janus particles comprising native polystyrene spheres with a gold cap of ~50% area coverage (i.e., a Janus cap). In summary, Janus particles were fabricated by depositing a thin layer of gold in a physical vapor deposition system via thermal evaporation technique on one hemisphere of native poly-

styrene beads (Figure 1A,B). Following the gold coating process, a particle of interest was locally coated with carbon (Figure 1C). Local measurements were achieved by cutting away a portion of the Janus particle with a focused ion beam (FIB) to reveal the Janus particle cross-section (Figure 1D). The cut furnished an SEM micrograph from which the direct measure of gold thickness along the surface was possible. Although the techniques employed in our work (i.e., SEM, FIB) are not new, the application of these techniques, implementation, and analysis of this specific Janus particle system are new and important to the prediction and measurement of Janus particle dynamics.<sup>20</sup> Our measurements show that caps are not of constant thickness but rather varied in thickness along the contour of the gold cap. We also found

that varying deposition rates between 0.5 and 2 Å/s did not significantly impact the variation in thickness across the cap.

Molecular Probes polystyrene sulfate latex beads 5 µm in diameter were obtained from Fisher Scientific (lot #1964358). The polystyrene beads were drop cast onto 5 mm × 5 mm silicon wafers obtained from SPI supplies (lot #1200724). Silicon chips with the deposited monolayer of polystyrene particles were transferred onto a precut microscope slide with high-temperature adhesive tape. The samples were then transferred into a N2 filled glovebox via an antechamber. From the glovebox, the microscope slides holding the samples were secured to a metallic plate using screws. The plate was introduced into a physical vapor deposition system (Angstrom EvoVac), and rotated to orient the samples facing downward. The deposition system was pumped down to a base pressure of 4 x 10<sup>-6</sup> Torr, and gold was then deposited by thermal evaporation at the prescribed rate, thickness, and power (Figure 1E). The nominal thickness of the deposited material was tracked by a quartz crystal microbalance.

Following addition of the gold layer, the samples were transferred to an FEI Helios 650 Field Emission Scanning Electron Microscope with FIB. Carbon was locally deposited with the electron beam using an in situ gas injecting system (GIS) to protect the surface before ion beam cutting. Carbon was used rather than the default Pt to enhance the contrast of the gold in the image, as seen by the thin rectangular layer surrounding the particle (Figure 1F). The additional carbon layer also helped to protect the thin gold layer from delamination during the subsequent FIB cut. A 16 kV 0.43 nA ion-beam current was used with the FIB to mill away layers to reveal the cross-section of the particle (Figures 1G,H). Finally, the particle was imaged at an angle of  $\theta = 52^{\circ}$  (angle in which the particles are normal to the ion beam) to visualize the gold layer thickness. The tilt angle of the sample impacted the interpretation of the imaged thickness. The extent of the impact depended on the angular  $\phi$  position of the measurement because only distances in the y-axis required correction (Figures S1-S4). SEM images revealed the gold coating as a thin line of bright pixels on the top perimeter of the particle. Images were processed to determine the local thickness of the bright line.

Initially, the mean and standard deviation of pixel depth along the gold cap was determined at three locations ( $\phi$  = 135°, 90°, 45°) to obtain a threshold value  $I_t$  that would eliminate any nongold pixels (Figure 2). The threshold value was set equal to the difference of the mean  $I_{\rm m}$  and standard deviation s of the pixel depth found along the gold cap ( $I_t = I_m$ -s). Once the threshold value was determined, the 8-bit SEM image was made binary, leaving behind an image with a black background (pixel depth = 0), cap (pixel depth = 255), and stray pixels (pixel depth = 255). Stray pixels were a consequence of portions of the top of the particle having brightness equal to or greater than that of the gold perimeter (Figure S2). Once a binary image was obtained, the thickness of the cap was measured with a custom macro written for Fiji (https://fiji.sc/). An ellipse was fit to the curve representing the cap because the spherical particle appeared as an ellipse as the sample was imaged at an angle (Figure S4). The pixel depth was then measured along a line from the center of the ellipse to a point closely (40–50 pixels from center of contour) outside that of the cap. Intensity profile curves were then analyzed to pinpoint the location of the boundary between the core polystyrene particle and the gold metal cap by identifying

the portion of the curve that possesses a pixel depth of zero for each particular angle  $\phi$  and repeating the measurement along 1000 profiles from  $\phi = 0^{\circ}$  to 180°. Included in this measurement was a requirement that a pixel was counted as gold if and only if three pixels in a row had a depth greater than or equal to  $2 \times 255 = 510$ . Thus, single dark pixels with two bright neighbors count but a dark pixel with one bright neighbor and one dark neighbor would not count as gold. This requirement included dropped pixels in the cap interior but excluded stray pixels outside the cap. Finally, the actual length was determined by converting the pixel number counted as gold (integer number of pixels) to real thickness (nm) while accounting for the image tilt. The pixel resolution varied slightly depending on the imaging conditions from 1.04 to 1.67 nm/pixel. The specific processing procedure used herein identified the cap to the level of a pixel, meaning the limiting resolution of our result is ~1 nm. Note that increased resolution of this technique may be achievable by utilizing additional image processing steps often used in particle tracking to achieve subpixel accuracy.<sup>21</sup>

The image processing and measurements were conducted for Janus particles prepared with nominal thicknesses of 10 or 20 nm at fixed deposition rates of 0.5, 1, and 2 Å/s. Figure 3

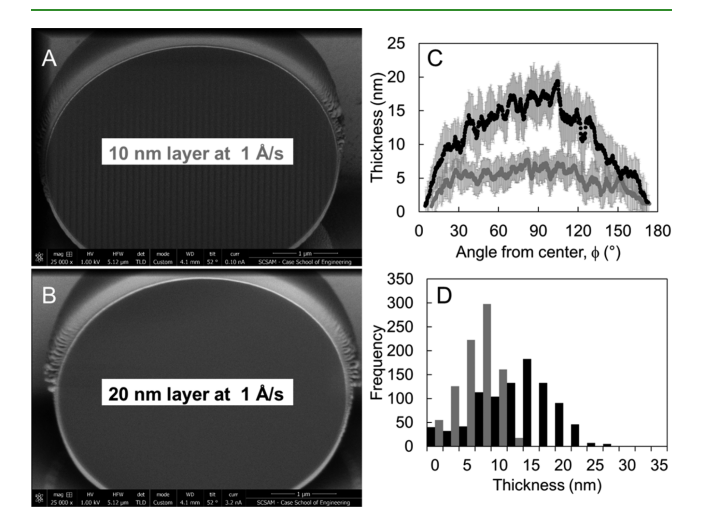


Figure 3. Thickness measurement for two thicknesses at fixed rate: 5  $\mu$ m polystyrene spheres with a gold cap of nominal thickness (A) 10 and (B) 20 nm deposited at 1 Å/s. (C,D) The gold thickness varied continuously over the contour for both the 10 and 20 nm caps. Solid black and solid gray points and bars are for 20 and 10 nm layers, respectively.

shows the SEM micrographs, measured thicknesses along the contour, and histogram of thicknesses for 20 nm caps deposited at 1 Å/s. The measured thicknesses were reported as moving averages for every 20 measurements (Figure 3C), and the histogram was assembled for every thickness measurement (1000 total between  $\phi = 0^{\circ}$  and  $180^{\circ}$ ). The cap thickness varied continuously along the contour of the particle between  $\sim 0$  nm at the equator ( $\phi = 0^{\circ}$  and  $180^{\circ}$ ) to a maximum near the pole ( $\phi = 90^{\circ}$ ). The maximum and mean thickness of all measurements, prior to taking moving average as shown in Figure 3, with standard deviation were 29.57 and  $11.84 \text{ nm} \pm 5.77 \text{ nm}$  for the 20 nm cap and 11.87 and 5.00 nm $\pm$  2.68 nm for the 10 nm cap. Surfaces normal to the deposition source had a thickness nearly matching the prescribed nominal thickness, whereas surfaces deviating

**ACS Applied Materials & Interfaces** 

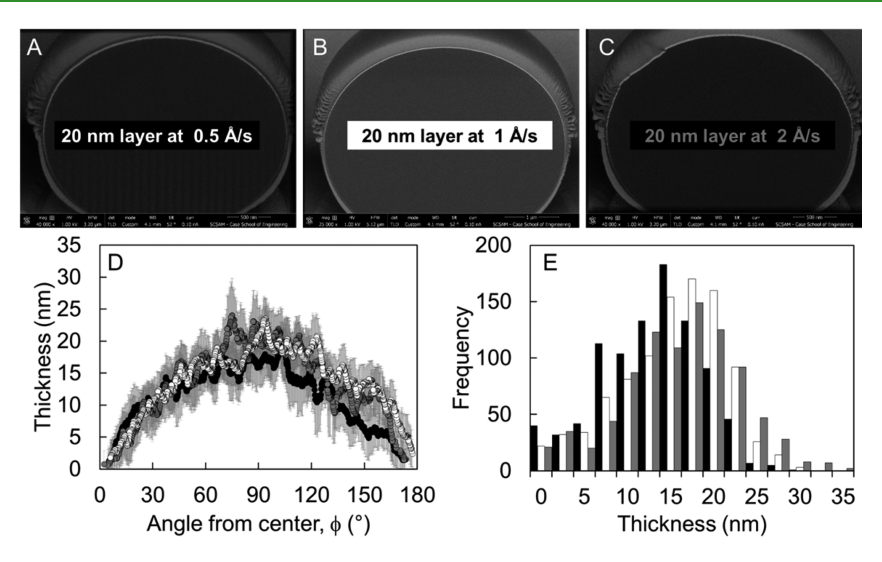


Figure 4. Thickness measurement for nominal 20 nm thickness at three different rates:  $5 \mu m$  polystyrene spheres with a gold cap of thickness 20 nm deposited at (A) 0.5, (B) 1.0, and (C) 2.0 Å/s. (D) The gold thickness varied continuously over the contour for each sample but did not show any impact of deposition rate in this range. (E) A histogram of thicknesses did not reveal significant differences as a consequence of deposition rate. White points with black outline, solid black, and gray points with black outline are for 0.5, 1.0, and 2.0 Å/s, respectively.

from normal had a thickness less than that of the nominal thickness, approaching ~0 nm when the surface was perpendicular. Cap thickness varying across the gold contour was an anticipated result with this variation being previously suggested as an explanation for observed deviations in experimental systems from the predicted behavior for a perfect Janus cap.<sup>2</sup>

A second set of experiments was conducted to test the impact of deposition rate on the variation in thickness across a Janus cap. Particles were prepared with nominally 20 nm thick caps at rates of 0.5, 1, and 2 Å/s. Figure 4 shows SEM images of cross sections of these particles under these conditions, thickness profiles, and histograms of thickness measurements for the three conditions. Similar to data summarized in Figure 3, Figure 4 shows strong variation in cap thickness along the contour of the particle. However, there were no perceptible differences between caps deposited at the rates chosen either in the coarse variation of cap thickness or in the local roughness. The histograms show very similar distributions with mean thicknesses and standard deviations of 14.02  $\pm$  6.01, 11.84  $\pm$ 5.77, and 14.66  $\pm$  6.66 nm for 0.5, 1, and 2 Å/s, respectively.

In summary, we presented an experimental and image processing procedure to measure the local cap thickness of Janus particles consisting of a 5  $\mu$ m native polystyrene particle with a gold cap. Our data show cap thickness strongly varies over the contour of the cap and that deposition speeds between 0.5 to 2 Å/s do not significantly alter this thickness variation or roughness of deposited material. These data can be used to accurately model the thickness of the cap for experiments or simulations that are concerned with the dynamics of a Janus particle at equilibrium or in response to external fields. Most work concerned with Janus particles has assumed a uniform coating thickness. However, nonuniform coverage (as detailed herein) will impact the rotational and translational dynamics of a Janus particle in different environments. Note that this work was done only on one slice to demonstrate a proof of concept for imaging the Janus layer. It would be possible to image and assemble a full 3D model of the cap by using the "slice and view" method. 23-25 Slice and view is an automated protocol for conducting serial

sectioning of the sample, where each feature of interest is traced to create a 3D model of the cap.

#### ASSOCIATED CONTENT

# S Supporting Information

The Supporting Information is available free of charge on the ACS Publications website at DOI: 10.1021/acsami.8b11011.

Figures detailing the image processing used to obtain cap measurement: SEM micrograph of a 5  $\mu$ m polystyrene bead with 20 nm cap deposited at 1 Å/s, binary SEM micrograph of 5  $\mu$ m polystyrene bead with 20 nm cap deposited at 1 Å/s following a threshold of 150, example line along which intensity was measured, illustration showing particle inclinations inside the FEI Helios 650 Field Emission Scanning Electron Microscope after carbon coating and cutting of the particle (PDF)

### AUTHOR INFORMATION

#### **Corresponding Author**

\*E-mail: c.wirth@csuohio.edu.

Ina T. Martin: 0000-0001-9452-3299

Christopher L. Wirth: 0000-0003-3380-2029

The authors declare no competing financial interest.

## **ACKNOWLEDGMENTS**

This work was supported by the Cleveland State University Office of Research Startup Fund and Graduate Student Research Award (AR), the National Science Foundation CAREER Award no. 1752051, and an Undergraduate Summer Research Award (MWI). Acknowledgment is made to the Donors of the American Chemical Society Petroleum Research Fund for partial support of this research.

#### REFERENCES

- (1) Zhang, J.; Luijten, E.; Granick, S. Toward Design Rules of Directional Janus Colloidal Assembly. *Annu. Rev. Phys. Chem.* **2015**, 66 (1), 581–600.
- (2) Ding, H.; Ma, Y. Interactions between Janus Particles and Membranes. *Nanoscale* **2012**, *4* (4), 1116–1122.
- (3) Crossley, S.; Faria, J.; Shen, M.; Resasco, D. E. Solid Nanoparticles That Catalyze Biofuel Upgrade Reactions at the Water/Oil Interface. *Science (Washington, DC, U. S.)* **2010**, 327 (5961), 68–72.
- (4) Tu, F.; Lee, D. Shape-Changing and Amphiphilicity-Reversing Janus Particles with PH-Responsive Surfactant Properties. *J. Am. Chem. Soc.* **2014**, *136* (28), 9999–10006.
- (5) Bahrami, R.; Löbling, T. I.; Gröschel, A. H.; Schmalz, H.; Müller, A. H. E.; Altstädt, V. The Impact of Janus Nanoparticles on the Compatibilization of Immiscible Polymer Blends under Technologically Relevant Conditions. ACS Nano 2014, 8 (10), 10048–10056.
- (6) Tu, F.; Lee, D. One-Step Encapsulation and Triggered Release Based on Janus Particle-Stabilized Multiple Emulsions. *Chem. Commun.* **2014**, *50* (98), 15549–15552.
- (7) Walther, A.; Müller, A. H. E. Janus Particles: Synthesis, Self-Assembly, Physical Properties, and Applications. *Chem. Rev.* **2013**, *113* (7), 5194–5261.
- (8) Zarzar, L. D.; Sresht, V.; Sletten, E. M.; Kalow, J. A.; Blankschtein, D.; Swager, T. M. Dynamically Reconfigurable Complex Emulsions via Tunable Interfacial Tensions. *Nature* **2015**, *518* (7540), 520–524.
- (9) Zhang, J.; Grzybowski, B. A.; Granick, S. Janus Particle Synthesis, Assembly, and Application. *Langmuir* **2017**, 33 (28), 6964–6977.
- (10) Chaudhary, K.; Chen, Q.; Juárez, J. J.; Granick, S.; Lewis, J. A. Janus Colloidal Matchsticks. J. Am. Chem. Soc. 2012, 134 (31), 12901–12903.
- (11) De Leon, A. C.; Rodier, B. J.; Luo, Q.; Hemmingsen, C. M.; Wei, P.; Abbasi, K.; Advincula, R.; Pentzer, E. B. Distinct Chemical and Physical Properties of Janus Nanosheets. *ACS Nano* **2017**, *11* (7), 7485–7403
- (12) Binks, B. P.; Lumsdon, S. O. Influence of Particle Wettability on the Type and Stability of Surfactant-Free Emulsions †. *Langmuir* **2000**, *16* (23), 8622–8631.
- (13) Du, Z.; Bilbao-Montoya, M. P.; Binks, B. P.; Dickinson, E.; Ettelaie, R.; Murray, B. S. Outstanding Stability of Particle-Stabilized Bubbles. *Langmuir* **2003**, *19* (8), 3106–3108.
- (14) Binks, B. P.; Lumsdon, S. O. Pickering Emulsions Stabilized by Monodisperse Latex Particles: Effects of Particle Size. *Langmuir* **2001**, *17* (15), 4540–4547.
- (15) Ergun, R.; Hartel, R. W.; Spicer, P. T. Kinetic Effects on Interfacial Partitioning of Fat Crystals. *Food Struct.* **2015**, *5*, 1–9.
- (16) Takei, H.; Shimizu, N. Gradient Sensitive Microscopic Probes Prepared by Gold Evaporation and Chemisorption on Latex Spheres. *Langmuir* **1997**, *13* (7), 1865–1868.
- (17) Pawar, A. B.; Kretzschmar, I. Multifunctional Patchy Particles by Glancing Angle Deposition. *Langmuir* **2009**, *25* (16), 9057–9063.
- (18) Pawar, A. B.; Kretzschmar, I. Patchy Particles by Glancing Angle Deposition. *Langmuir* **2008**, 24 (2), 355–358.
- (19) Pawar, A. B.; Kretzschmar, I. Fabrication, Assembly, and Application of Patchy Particles. *Macromol. Rapid Commun.* **2010**, *31* (2), 150–168.
- (20) Rashidi, A.; Wirth, C. L. Motion of a Janus Particle Very near a Wall. *J. Chem. Phys.* **2017**, *147* (22), 224906.
- (21) Crocker, J.; Grier, D.; Crocker, J.; Grier, D. Methods of Digital Video Microscopy for Colloidal Studies. *J. Colloid Interface Sci.* **1996**, 179 (1), 298–310.
- (22) Wang, X.; In, M.; Blanc, C.; Würger, A.; Nobili, M.; Stocco, A. Janus Colloids Actively Rotating on the Surface of Water. *Langmuir* **2017**, 33 (48), 13766–13773.
- (23) Avishai, A.; Yin, X.; Trapp, B.; Kidd, G. Focused Ion Beam-Based Three Dimensional Analysis of Optic Nerve Axons. *Microsc. Microanal.* **2009**, *15* (S2), 346–347.

- (24) Mustafi, D.; Avishai, A.; Avishai, N.; Engel, A.; Heuer, A.; Palczewski, K. Serial Sectioning for Examination of Photoreceptor Cell Architecture by Focused Ion Beam Technology. *J. Neurosci. Methods* **2011**, *198* (1), 70–76.
- (25) Kidd, G.; Avishai, A.; Yin, X.; Trapp, B. Three-Dimensional Analysis of Optic Nerve Axons Using a Focused Ion Beam-Based Appraoch. *Microsc. Today* **2010**, *18*, 18–22.